

# COLLAPSE OF LIGHTLY CONFINED REINFORCED CONCRETE FRAMES DURING EARTHQUAKES

JACK P. MOEHLE\*, WASSIM GHANNOUM, AND YOUSEF BOZORGNIA  
*Pacific Earthquake Engineering Research Center, University of California, Berkeley,  
USA*

**Abstract.** Post earthquake studies show that the primary cause of reinforced concrete building collapse during earthquakes is the loss of vertical-load-carrying capacity in critical building components leading to cascading vertical collapse, rather than loss of lateral-load capacity. In cast-in-place beam-column frames, the most common cause of collapse is failure of columns, beam-column joints, or both. This study emphasizes failure of columns using data from laboratory studies. Failure models are incorporated in nonlinear dynamic analysis software, enabling complete dynamic simulations of building response including component failure and progression of collapse. This approach enables more realistic simulation of building collapse than is possible using simplified assessment procedures, and provides insight into the conditions that cause collapse and the variability of collapse as a function of input ground motions.

## 1. Introduction

Post earthquake studies show that the primary cause of reinforced concrete building collapse during earthquakes is the loss of vertical-load-carrying capacity in critical building components leading to cascading vertical collapse, rather than loss of lateral-load capacity. In cast-in-place beam-column frames, the most common cause of collapse is failure of columns, beam-column joints, or both. Once axial failure occurs in one or more components, vertical loads arising from both gravity and inertial effects are transferred to adjacent framing components. The ability of the frame to continue to support vertical loads depends on both the capacity of the framing system to transfer these loads to adjacent components and the capacity of the adjacent components to support the additional load. When one of these conditions is deficient, progressive failure of the building can ensue.

Post-earthquake reconnaissance of reinforced concrete buildings provides some insight into the prevalence of collapse among populations of heavily shaken buildings. Otani (1999) reports damage statistics of reinforced concrete buildings, with damage defined in three categories:

- 1. Operational damage (light to minor damage): columns or structural walls were slightly damaged in bending, and some shear cracks might be observed in non-structural walls;
- 2. Heavy damage (medium to major damage): spalling and crushing of concrete, buckling of reinforcement, or shear failure in columns were observed, and lateral resistance of shear walls might be reduced by heavy shear cracking; and
- 3. Collapse (partial and total collapse), which also included those buildings demolished at the time of investigation.

---

\* moehle@berkeley.edu

Figure 1.1 presents the distribution of damage for four earthquakes reported by Otani (1999). For the 1985 Mexico earthquake, data are restricted to the lakebed zone of Mexico City; for the 1990 Luzon, Philippines earthquake, data are from Baguio City; for the 1992 Erzincan, Turkey earthquake, data are from two heavily damaged residential areas of Erzincan; and for the 1995 Kobe earthquake, data are from areas of highest seismic intensity in Kobe and restricted to buildings constructed before enforcement of the 1981 Building Standard Law. Figure 1.1 shows that even in areas of highest damage in famously damaging earthquakes, the collapse rates of lightly detailed reinforced concrete buildings are relatively low.

Given the relatively low collapse rate shown in Figure 1.1, it is reasonable to conclude that refined engineering tools might be useful to identify those buildings that are most collapse prone, so that resources could be focused on seismic mitigation of those buildings. By reducing the number of buildings urgently requiring retrofit from a large number to a small fraction of that number, mitigation programs that are stymied by huge retrofit costs may become more tractable. Ultimately, this is one of the main objectives of this work reported here.

Small steps have been made toward the development and implementation of refined engineering tools for building response simulation near and beyond the collapse initiation stage. Laboratory studies of reinforced concrete columns with light transverse reinforcement have identified primary variables that contribute to loss of column axial-load capacity. These models have been implemented in nonlinear dynamic analysis software that can be used to simulate building collapse during earthquake shaking. In one example, the software is used in a limited study to simulate building response to a series of strong ground motions recorded within a relatively small region during the 1994 Northridge earthquake. The results provide some insight into the collapse of building frames as well as the influence of local ground motion on collapse. The following text details some of these developments.

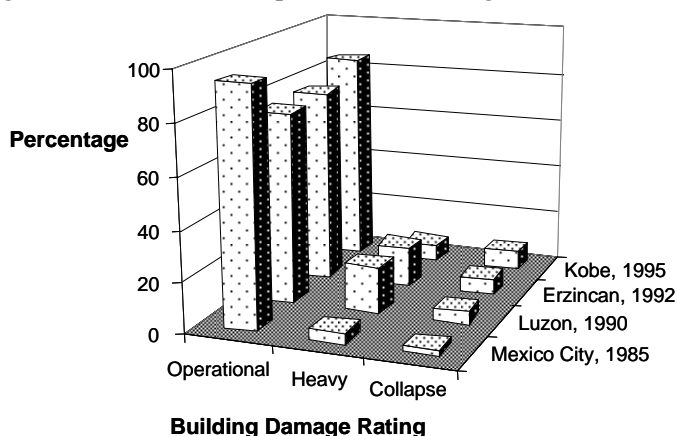


Figure 1.1 Damage statistics from four earthquakes

## 2. Shear and Axial Load Failure of Reinforced Concrete Columns

Of primary interest in this study is the behavior of reinforced concrete columns with relatively light transverse reinforcement and with proportions that enable the column to yield in flexure prior to developing shear or axial failure. Columns with these details and proportions may be able to sustain moderately large lateral deformations prior to failure; a challenge is to estimate the lateral drift at which failure occurs.

For a column that yields in flexure, the lateral strength is limited to the flexural strength, and therefore can be calculated with relatively high accuracy. The column may subsequently sustain apparent shear failure. Although the details of the mechanism leading to shear failure are not fully understood, it is postulated that crack opening and tensile straining reduce the shear-carrying capacity of the concrete through loss of aggregate interlocking but primarily excessive strain demand on the compression zone, while spalling and bond distress lead to degradation of the transverse reinforcement

contribution. To identify whether shear failure is likely, it is necessary to estimate whether the shear strength will degrade to a value approaching the flexure strength.

Sezen and Moehle (2004) report a model for shear strength of columns that initially yield in flexure. The empirical model is based on theoretical concepts of shear resistance but is calibrated to test data. The shear strength is defined as

$$V_n = V_s + V_c = k \frac{A_{st} f_{yt} d}{s} + k \left( \frac{0.5 \sqrt{f'_c}}{a/d} \sqrt{1 + \frac{P}{0.5 \sqrt{f'_c} A_g}} \right) 0.8 A_g \quad (\text{MPa}) \quad (1)$$

where  $V_s$  and  $V_c$  are shear contributions assigned to steel and concrete;  $k$  is a parameter equal to 1 for  $\mu_\delta \leq 2$ , equal to 0.7 for  $\mu_\delta \geq 6$ , and varies linearly for intermediate  $\mu_\delta$  values;  $\mu_\delta$  = displacement ductility;  $A_{st}$  = area of shear reinforcement parallel horizontal shear force within spacing  $s$ ;  $f_{yt}$  = yield strength of transverse reinforcement;  $d$  = effective depth ( $=0.8h$ , where  $h$  = section depth parallel shear force);  $P$  = axial compression force;  $f'_c$  = concrete compressive strength (MPa);  $A_g$  = gross section area, and  $a/d$  = shear span/effective depth (value limited between 2 and 4). Figure 2.1 compares measured and calculated shear strengths. The mean ratio of measured to calculated strength and its coefficient of variation are 1.06 and 0.15.

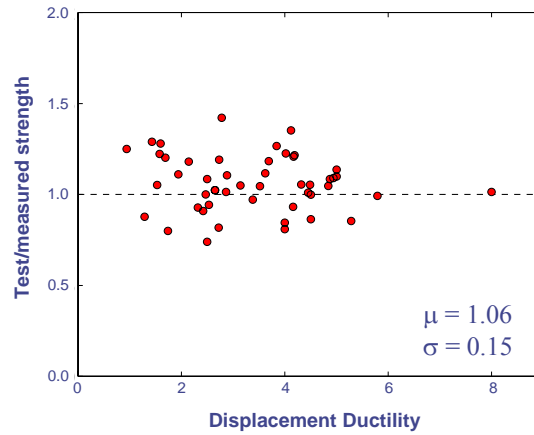


Figure 2.1 Ratios of strengths measured during tests to strengths calculated by the strength model

If shear strength degrades to below flexure strength, shear failure is anticipated. Elwood and Moehle (2004) developed an empirical model to estimate deformation at shear failure using the same data as shown in Figure 2.1. For this model, shear failure was defined as the loss of twenty percent of the maximum shear strength. The data show that deformation at shear failure decreases with increasing shear stress, increasing axial stress, and decreasing transverse reinforcement index. According to the model, deformation at shear failure is defined as

$$\frac{\delta_s}{L} = \frac{3}{100} + 4\rho'' - \frac{1}{40} \frac{v}{\sqrt{f'_c}} - \frac{1}{40} \frac{P}{A_g f'_c} \geq \frac{1}{100} \quad (\text{MPa}) \quad (2)$$

where  $\rho''$  = transverse steel ratio and  $v$  = nominal shear stress. Figure 2.2 compares results from tests and from Equation (2). The mean ratio of measured to calculated strength and its coefficient of variation are 0.97 and 0.34.

Axial load failure may coincide with onset of shear failure or may occur at larger drift. Elwood and Moehle (2004) use concepts of shear-friction and experimental data to derive an expression for the drift at axial load failure of columns initially yielding in flexure, then developing shear failure, and finally developing axial failure. The drift at shear failure is estimated as

$$\delta_a = \frac{4}{100} \frac{1 + \tan^2 \theta}{\tan \theta + P \left( \frac{s}{A_{st} f_{yt} d_c \tan \theta} \right)} \quad (3)$$

in which  $\theta$  = critical crack angle (assumed = 65 deg) and  $d_c$  = depth of the column core measured parallel to the applied shear. Figure 2.3 compares results of tests and Equation (3).

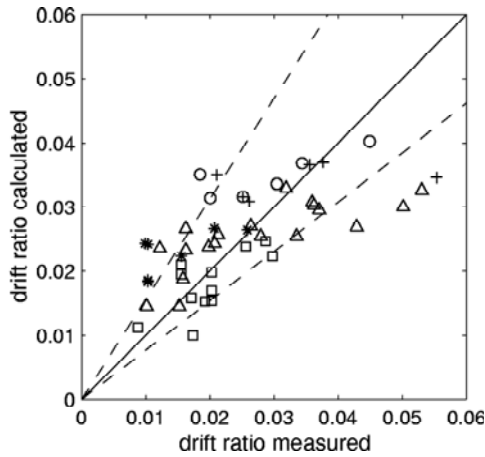


Figure 2.2 Displacement capacity measured and calculated by Equation (2)

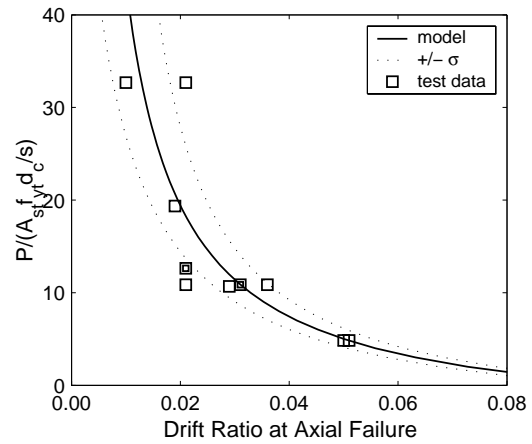


Figure 2.3 Drift capacity curve based on shear-friction model

It is important to note that the models presented were for columns with rectangular cross section, relatively light and widely spaced transverse reinforcement, subjected to unidirectional lateral load. Additional data are needed to validate models for other conditions

### 3. Implementation of Axial Failure Model in OpenSees

Shear and axial failures were modeled in OpenSees by adding at the end of the columns zero-length Limit State spring elements developed by Elwood (2002) (Figure 3.1). These elements have differing backbone curves before and after failures are detected. Prior to shear failure, the shear springs are elastic with stiffness corresponding to the shear stiffness of the column. Once the element reaches the limit curve defined by an empirical shear-drift relation (Elwood 2002) the shear spring backbone curve is modified to a degrading hysteretic curve (Figure 3.2). The shear degrading slope  $K_{deg}$  is calibrated based on observations from previous tests (Nakamura and Yoshimura, 2002), which have shown that axial failure is initiated when shear strength degrades to about zero.

Similarly, the zero-length axial springs have a “rigid” backbone prior to reaching the axial load-drift limit curve (Elwood 2002) (Figure 3.2). This limit curve is defined by the shear-friction model and, hence, assumes that shear failure has already occurred in the element. Once the column element reaches that drift limit curve its axial load-vertical deformation backbone is modified to a degrading hysteretic material model. Because the shear-friction model only describes compression failures, the backbone is only redefined for compressive axial loads. Beyond the initiation of axial failure, a coupling effect exists between the horizontal and vertical deformations where an increase in horizontal drift causes an increase in vertical deformation. This effect is modeled in the vertical spring element with an iterative procedure that keeps the column response on the horizontal drift-axial load curve defined by the shear-friction model. When the earthquake motion reverses direction, the vertical spring backbone is redefined to an elastic response with a reduced elastic stiffness to account for the damage in the column. This modification also halts the axial degradation in the column as it is assumed that the critical shear crack closes which prevents any further sliding along that crack.

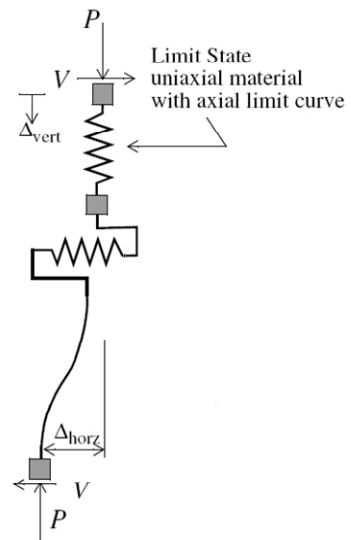


Figure 3.1 Zero-length springs

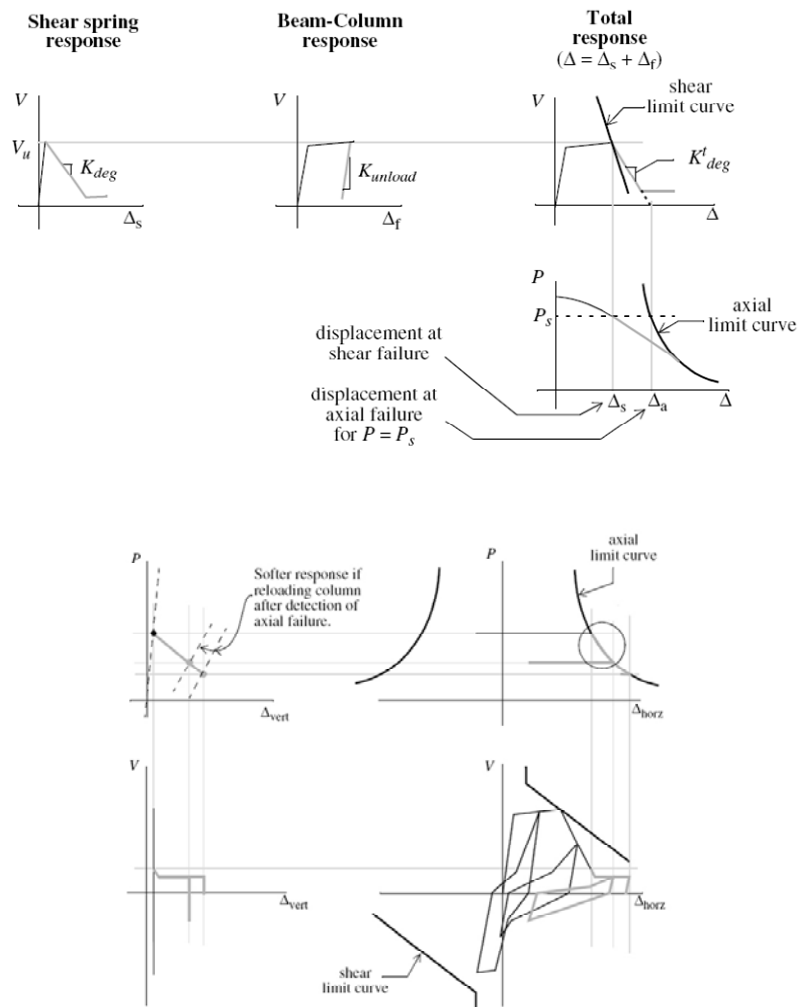


Figure 3.2 Shear and axial zero-length element responses and limit curves (Elwood 2002)

## 4. Study of the Dynamic Response of a Building Frame

### 4.1. BUILDING FRAME DESCRIPTION

As an illustration of the use of the models and implementation described previously, a 3-bay, 3-story RC frame was analyzed for a series of different ground motions. The building frame was dimensioned to represent typical 1960s and 1970s office building construction in California. The building frame (Figure 4.1) was designed for third-scale shake-table testing at the University of California, Berkeley under an ongoing research effort aimed at understanding non-ductile RC frame collapse mechanisms. Two of the columns in this frame have non-ductile detailing with widely spaced ties, 90° hooks, and no ties in the joints, while the other two columns have ductile detailing as per ACI 318-2002 recommendations. The ductile columns are to better control the collapse of the structure during shake-table testing.

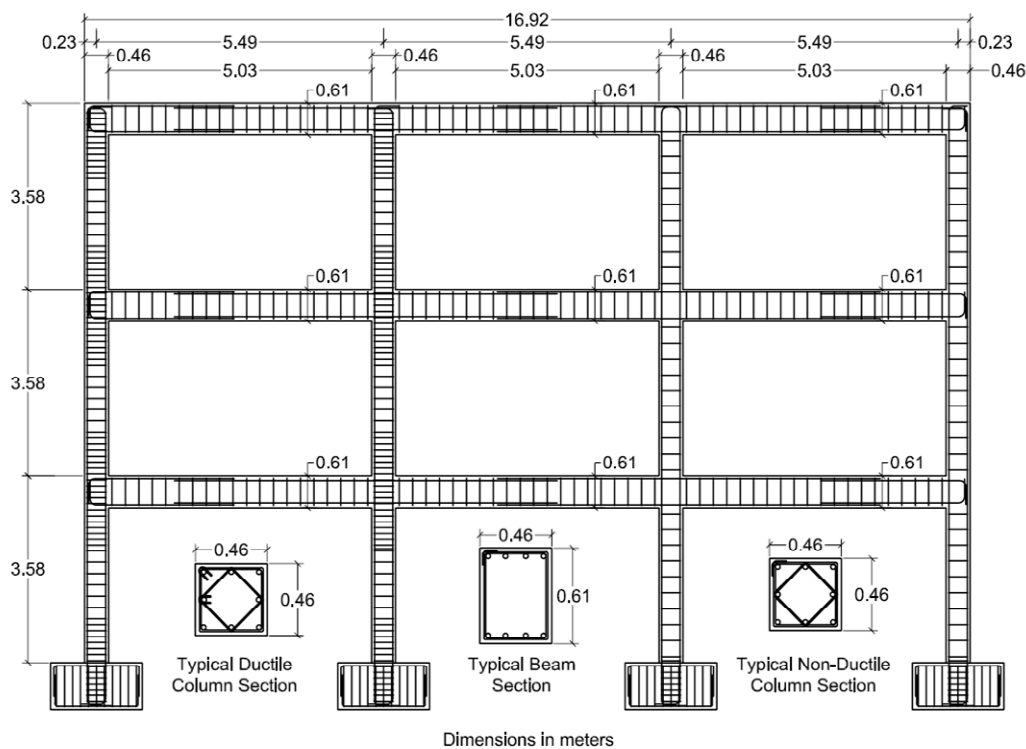


Figure 4.1 Frame details

Beam depth and reinforcement were chosen to create a weak-column strong-beam mechanism as well as to reduce joint shear stresses. The resulting concentration of damage in the non-ductile columns is intended to force axial collapse in these columns at high drifts. The beam reinforcement details are typical of those in moment-resisting frames built in the 1960s and 1970s in California.

Masses added to the frame for the dynamic analysis are equivalent to those expected considering dead loads for a two-way slab system typical of office building construction. The masses result in approximately  $0.1A_g f'_c$  axial load on the first-floor center columns. The resulting structure has initial elastic first-mode period of 0.60 sec.

Target concrete cylinder strength  $f'_c$  is 24.6 MPa and target steel yield strength  $f_y$  is 486 MPa. Concrete is modeled in OpenSees using the concrete01 uniaxial material model (Kent-Scott-Park model with a degraded unloading/ reloading stiffness according to Karsan and Jirsa). Concrete is modeled with no tension strength. Steel is modeled using the steel01 model (bilinear with kinematic hardening). Flexure, shear and axial effects of components were modeled, and slip of longitudinal reinforcement from joints was considered using rotational springs at column and beam ends. Effects of splices were not modeled.

#### 4.2. SELECTED EARTHQUAKE GROUND MOTIONS

The structural model is subjected to seven ground accelerations recorded during the 1994 Northridge, California, earthquake. By choosing the records from a single earthquake, the earthquake-to-earthquake variability of ground motions is excluded from the analysis. Additionally, by selecting a set of recording sites located in the same general area, spatial variability of the recorded ground motion is relatively reduced. The selected strong motion recording stations are listed in Table 1.

The locations of the recording stations, along with the epicenter and the surface projection of the fault rupture plane are mapped in Figure 4.2. As provided in Table 1, the selected recording stations constitute a closely spaced cluster of sites located between 5.19 and 6.5 km from the fault plane. The sites have either NEHRP site class 'C' or 'D'. The shear-wave velocity in the top 30-meter of soil is in the range of 251 to 441 m/s (see Table 1).

Figure 4.3 shows 5% damped elastic response spectra of the horizontal ground motions at the selected sites. This figure shows the variability of the ground motion as elastic structural response is concerned. The effects of such variability on nonlinear dynamic response of the structural models will be discussed in the next section.

The site classifications at the recording stations, average shear-wave velocity at top 30-m of soil, various distance measures, and the processed ground motion records have been obtained from the recently enhanced and expanded PEER strong motion database. The expanded PEER ground motion database includes strong motion records at more than 3,000 stations recorded in more than 170 worldwide earthquakes from 1935 to 2003.

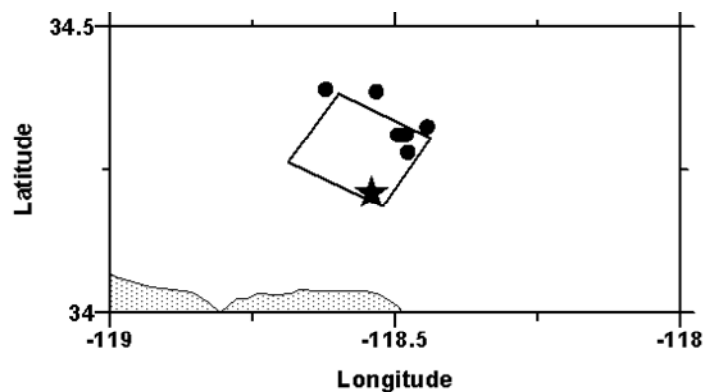


Figure 4.2 The 1994 Northridge, California, earthquake: epicenter (star symbol), surface projection of the fault plane, and locations of the selected recording stations (solid circles) are marked

TABLE 1. Strong ground motion records used in this study

station	$R_{seis}$ (km)	$R_{rup}$ (km)	NEHRP site class	$V_{s30}$ (m/s)	PGA (g)	PGV (cm/s)
Sylmar - Converter Sta East	6.20	5.19	C	370.52	0.64	93.60
Sylmar - Olive View Med FF	6.20	5.30	C	440.54	0.71	100.70
Sylmar - Converter Sta	6.30	5.35	D	251.24	0.74	109.90
Jensen Filter Plant	6.40	5.43	C	373.07	0.50	102.70
Newhall - W Pico Canyon Rd.	6.70	5.48	D	285.93	0.38	79.10
Newhall - Fire Sta	7.00	5.92	D	269.14	0.59	85.70
Rinaldi Receiving Sta	7.40	6.50	D	282.25	0.63	110.10

**Notes:**  $R_{seis}$  = Campbell & Bozorgnia distance to seismogenic portion of the fault plane

$R_{rup}$  = Distance to fault rupture plane

NEHRP = U.S. National Earthquake Hazard Reduction Program

$V_{s30}$  = Average shear-wave velocity in the top 30-meter of soil

PGA = Peak ground acceleration, geometric mean of the two horizontal components

PGV = Peak ground velocity, geometric mean of the two horizontal components

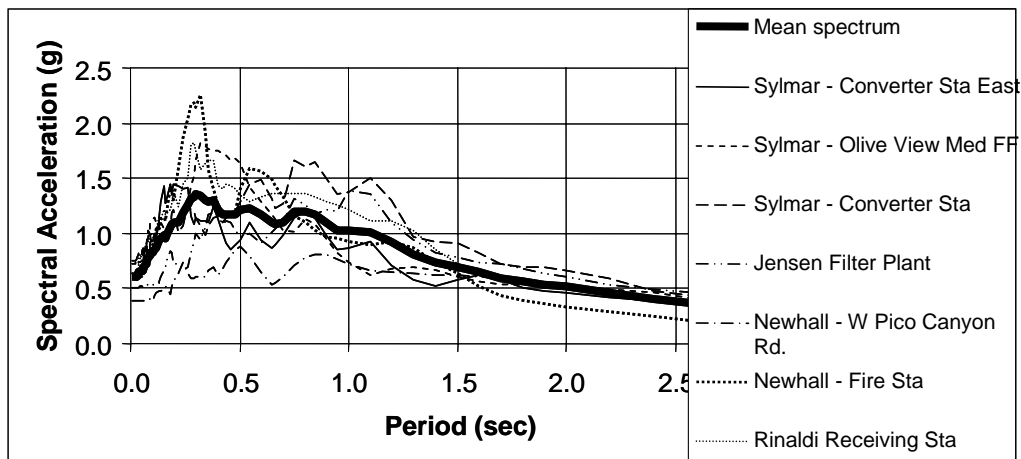


Figure 4.3 Response spectra for 5% damping of the selected 1994 Northridge records. The spectra are for the geometric mean of the two horizontal components.

#### 4.3. ANALYSIS RESULTS

Dimensioning and detailing of the frame were chosen to concentrate damage in the non-ductile columns at the first floor level, with little or no damage in the upper floor columns prior to collapse. A non-linear static analysis with a first-mode horizontal loading pattern was performed to identify the critical response and damage stages for the structure (Figure 4.4). The calculated response and damage sequence for the frame is as follows:

1. Yielding of all first floor column longitudinal steel occurs at a first floor horizontal drift of approximately 0.8%.
2. At approximately 2% horizontal drift, shear failures are initiated in the non-ductile columns.
3. Between approximately 2% and 7% horizontal drift, there is a gradual loss of shear capacity in the non-ductile columns until a residual shear/friction capacity is reached

4. At that drift level loss of axial load capacity in the non-ductile columns is initiated. It is important to note that these particular drift levels are mainly a function of the axial load on the columns.
5. As the structure is pushed to even higher drifts, it collapses on the non-ductile side of the frame dragging the ductile side with it. A drift of 8% on the first floor was deemed the collapse for this frame. This final stage can be altered by choosing “stronger” framing on the ductile side in which case only a partial collapse would have been observed.

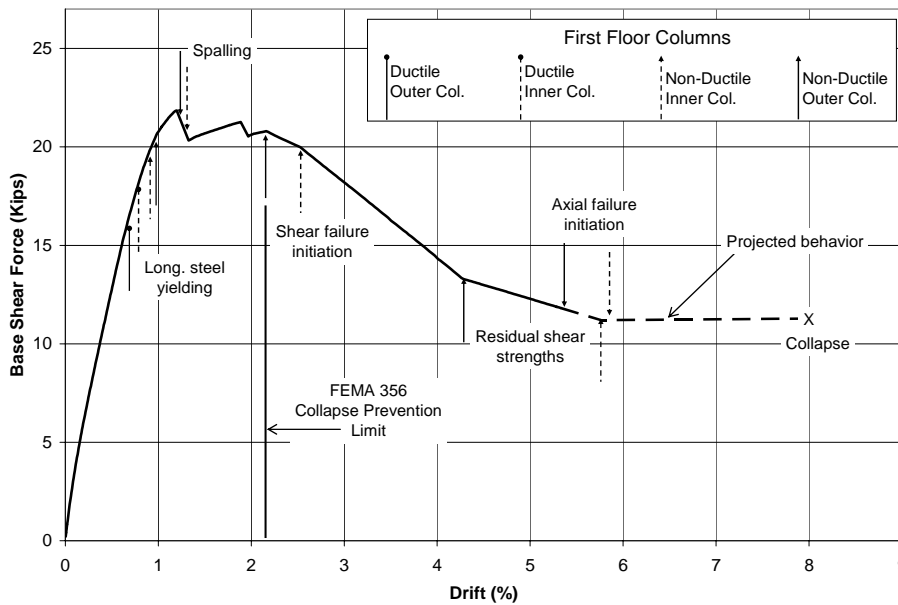


Figure 4.4 First-floor drift versus base-shear response

This displacement-controlled behavior prompted the use of the first floor drifts as the damage parameter for comparison among the different ground motion simulations. Figure 4.5 shows the first floor drift responses for the seven ground motions. Table 2 summarizes the maximum drift values as well as the behavior of the frame. The results summarized in Table 2 show tremendous variation in the frame responses when subjected to ground motions obtained from the same earthquake at sites of close proximity. These responses ranged from almost no yielding of the longitudinal steel to complete collapse of the frame.

It is evident here that local geological and soil conditions have significant effects on the earthquake response of a structure. As well, observing that the analysis results were obtained using the strongest directional component of the ground motions suggests that the orientation of the structure can have a significant effect on its response. This point was demonstrated with the SCS142 ground motion to which the frame was subjected in the East-West direction as well the West-East direction. For the EW direction which increased the axial load in the non-ductile columns at peak drift due to frame action, axial load carrying capacity degradation was calculated in these columns. As for the other direction, which imparted significant uplift on the non-ductile columns at peak drift, no axial degradation was calculated.

The dynamic analysis results (Figure 4.5) suggest that the response of any given building structure is rather sensitive to the details or the ground motion. Among populations of collapse-prone buildings, only a small fraction may sustain collapse in any given earthquake. Different earthquakes of similar scale but different detail may produce very different collapse scenarios. Thus, the small collapse rates of Figure 1.1 may not necessarily equate to equivalently small rates of seismic upgrading requirements. Upgrading of many buildings may be necessary if collapse mitigation is to be realistically achieved.

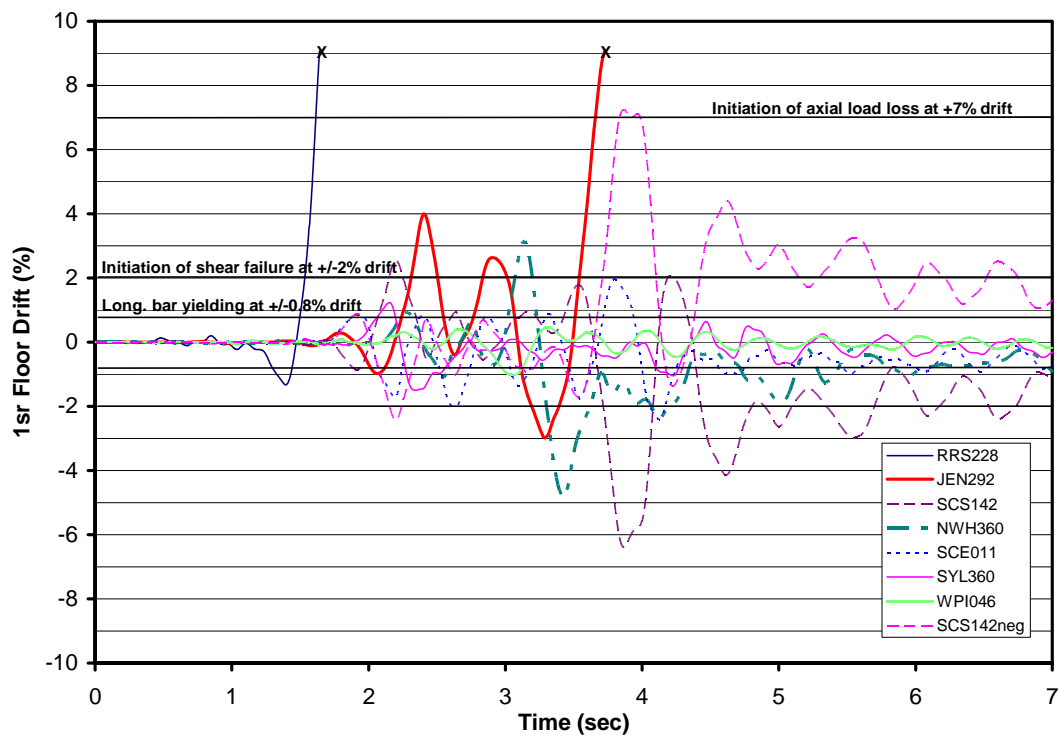


Figure 4.5 First-floor drift response history

Table 2: Summary table of first floor drifts and frame damage

Ground Motion	Max. / Min. 1 <sup>st</sup> Floor Drift	Damage
RRS228	> 9% / -1.3%	complete collapse of frame
JEN292	> 9% / -3.0%	complete collapse of frame
SCS142	2.5% / -6.4%	longitudinal steel yielding in all 1 <sup>st</sup> floor columns - shear failure up to residual in non-ductile 1 <sup>st</sup> floor columns - no axial load carrying capacity degradation
SCS142neg*	7.2% / -2.4%	longitudinal steel yielding in all 1 <sup>st</sup> floor columns - shear failure up to residual in non-ductile 1 <sup>st</sup> floor columns - axial load loss initiation in non-ductile 1 <sup>st</sup> floor columns – no collapse
NWH360	3.1% / -4.8%	longitudinal steel yielding in all 1 <sup>st</sup> floor columns - shear failure initiation with only partial degradation in non-ductile 1 <sup>st</sup> floor columns
SCE011	2.0% / -2.4%	longitudinal steel yielding in all 1 <sup>st</sup> floor columns - shear failure initiation with only slight degradation in non-ductile 1 <sup>st</sup> floor columns
SYL360	1.2% / -1.5%	longitudinal steel yielding in all 1 <sup>st</sup> floor columns
WPI046	0.5% / -1.0%	longitudinal steel just yielding in all 1 <sup>st</sup> floor columns

\* SCS142neg is the negative of the SCS142 ground motion (180° rotation)

It should be noted that the frame analysis software used here has relatively limited validation – therefore, the outcome of this analysis should be considered preliminary and only suggest the path forward. Additional shake-table tests are needed for validation of the software.

## 5. Conclusions

A model for shear and axial failure of lightly-confined reinforced concrete columns is developed for columns that sustain shear and axial failure following initial flexural yielding. Lateral strength can be estimated relatively accurately as the lateral force corresponding to flexural yield. Propensity for shear failure can be identified using a shear strength model in which shear strength following flexural yield degrades with increasing deformation demand. The drift at shear failure varies with transverse reinforcement amount and inversely with nominal axial and shear stresses. Drift at axial failure varies with transverse reinforcement and inversely with axial load.

The model is implemented in nonlinear dynamic analysis software to demonstrate the feasibility of conducting nonlinear dynamic analysis including shear and axial failure of columns. A three-story building model is subjected numerically to a series of ground motions recorded at stations located between 5.19 and 6.5 km from the fault plane of the 1994 Northridge earthquake. Response of the frame is found to be sensitive to the ground motions, with responses to individual ground motions varying from almost no yielding of longitudinal steel to total collapse. The results suggest that observed low collapse rates during strong earthquake shaking may not be reflective of small numbers of collapse-prone buildings but instead may be a manifestation of the vagaries of the ground motion. Experimental studies to validate the numerical results, and additional numerical studies to identify the characteristics of strong ground motion best correlated with collapse, are needed.

## 6. Acknowledgment

This work was supported by the Pacific Earthquake Engineering Research Center through the Earthquake Engineering Research Centers Program of the National Science Foundation under award number EEC-9701568. Any opinions, findings, and conclusions or recommendations expressed are those of the authors and do not necessarily reflect those of the National Science Foundation. Ground motion data were obtained from the PEER ground motion database (<http://peer.berkeley.edu>)

## References

- Elwood, K., and Moehle, J., 2005, "Drift Capacity of Reinforced Concrete Columns with Light Transverse Reinforcement," *Earthquake Spectra*, Earthquake Engineering Research Institute, Vol. 21, No. 1, pp. 71-89.
- Elwood, K., 2002, "Shake Table Tests and Analytical Studies on the Gravity Load Collapse of Reinforced Concrete Frames", Doctoral Dissertation, University of California, Berkeley.
- Elwood, K., and Moehle, J., 2004, "Evaluation of existing reinforced concrete columns," *Proceedings*, 13<sup>th</sup> World Conference on Earthquake Engineering, Vancouver.
- Nakamura, T., and Yoshimura, M., 2002, "Gravity Load Collapse of Reinforced Concrete Columns with Brittle Failure Modes", *Journal of Asian Architecture and Building Engineering*, Vol. 1, No. 1, pp. 21-27.
- OpenSees, 2004, *Open System for Earthquake Engineering Simulation*, <http://opensees.berkeley.edu>, Pacific Earthquake Engineering Research Center, University of California, Berkeley.
- Otani, S., 1999, "RC Building Damage Statistics and SDF Response with Design Seismic Forces", *Earthquake Spectra*, Earthquake Engineering Research Institute, Vol. 15, No. 3, pp. 485 - 501.
- Sezen, H., and Moehle, J., 2004, "Shear Strength Model for Lightly Reinforced Concrete Columns," H. Sezen and J. P. Moehle, *Journal of Structural Engineering*, ASCE, Vol. 130, No. 1692.